SCIENTIFIC CULTURE
www.sci-cult.com

SCIENTIFIC CULTURE, Vol. 10, No. 2, (2024), pp. 35-48
Open Access. Online & Print

DOI: 10.5281/zenodo.10621833

THE PYLOS GEOARCHAEOLOGICAL PROGRAM: FUSION OF IMAGES TOWARDS UNDERSTANDING ANCIENT LANDSCAPE

Alexandra Karamitrou[1,2], Maria Kylafi[3], Alexandros Stampolidis[1], Evangelia Militsi[3], Anastasios Kazolias[4], Gregory N. Tsokas[1], Vayia V. Panagiotidis[4]* and Nikolaos Zacharias[4]

[1]Laboratory of Exploration Geophysics, Aristotle University of Thessaloniki, Greece
[2]Department of Archaeology, University of Southampton, UK
[3]Ephorate of Antiquities, Ministry of Culture and Sports, 24133 Kalamata, Greece
[4]Laboratory of Archaeometry, Department of History, Archaeology and Cultural Management, University of the Peloponnese, 24100 Kalamata, Greece

Received: 18/01/2024
Accepted: 24/02/2024
Corresponding author: Vayia V. Panagiotidis (vpanagiotid@go.uop.gr)

ABSTRACT

The coastal zone in the northern area of Pylos, Messenia, constitutes a landscape of incomparable beauty and of particularly great historical, archaeological and environmental importance, while also providing for great tourist development. The windless ports of Navarino and Voidokoilia bay protected from the open sea by the long mountain ridges of the island of Sphakteria, the peninsula of Koryphasium including the hills of Prophitis Ilias and Koukouras in its northern edge, the access to the sea and therefore organised trade, the fertile hinterland attractive man who occupied the area from the Neolithic period (ca mid-4th millennium BC) and being active at intervals until nowadays leaving an impressive cultural reserve.

The five-year research program of "Pylos Geoarchaeological Program – GEAPP" is in operation since 2021. Among the goals of the Program that stand out are landscape reconstruction, the use of new technological tools for archaeological and environmental research, commitment to informing local bodies about the rich cultural heritage and the special ecosystem, while contributing to the balanced and sustainable development of the area.

The endeavour of the present study is an attempt to fuse data and images from a series of approaches, namely geophysical survey using magnetometry, aerial photography with the use of UAS and past excavation (since 1963) photos, implemented during the survey season of July 2021 covering an area of ca. 6,000m^2 North-East to the Profitis Elias hill at Pylos.

The co-evaluation of the geophysical data, remote sensing methods and surface research are targeting in maximizing the obtained information and increasing the reliability of the interpretation in the detection of archaeological targets. The results of the study provided the development of a technological case depended on methodology aiming to a better resolution and accuracy of the spotted antiquities and therefore towards a successful management of the area, safeguarding and promoting buried antiquities.

KEYWORDS: Pylos Geoarchaeological Program, geophysical prospection, LiDAR, remote sensing, aerial photogrammetry, data fusion, curvelet transformation models

1. RESEARCH AIMS - INTRODUCTION

The study presents a combination of remote sensing, geophysical and archaeological data aiming to improve the detectability of possible archaeological targets in the coastal region of Pylos located in SW Greece. The project explores the feasibility and practicality of combining images generated through different methods, magnetometry, satellite imagery, photogrammetry and LiDAR data, using various fusion techniques in order to merge all relevant information from the original images into a single image while minimizing background noise.

Remote Sensing and geophysical prospection are techniques widely used in archaeological exploration. Geophysical prospection methods found extensive application in the field of archaeological research producing images of subsurface layers providing archaeologists resourceful insights on the location of archaeological features using non-destructive methods (Tsokas et al., 2009; Vella & Sarris, 2022). Remote sensing including aerial and space borne imagery have introduced innovative non-invasive methods for archaeological research. Close range aerial photogrammetry using Unmanned Aerial Vehicles (UAVs) has become common practice over the past decade due to increased availability, low cost and satisfactory survey results producing high-resolution imagery increasing visibility for scientists (Panagiotidis & Zacharias, 2022; Nikolakopoulos et al., 2017). Similarly, Light Detecting and Ranging (LiDAR) laser scanners are also gaining ground in their application for aerial and terrestrial scanning in archaeological research increasing exponentially surface and ground presentation of areas of interest (Poirier et al., 2020; Risbøl & Gustavsen, 2018; Grammer et al., 2017).

These technologies and survey methods produce different imagery and data. Combining the various layers can be realized using different approaches. The advances in Machine learning (ML) algorithms for applications in image analysis have created an additional tool available in the study of archaeological sciences. This study presents the application of ML for the combination of the resulting data from the various remote sensing and geophysical techniques utilized during the Pylos Geoarchaeological Program during the 2021-2022 excavation period (Kadhim & Abed, 2023).

Aerial LiDAR scanning is a remote sensing technology that uses laser light to measure distances between the sensor and the target area on the ground. The sensor emits rapid pulses of laser light and records the time it takes for the light to return from the ground surface, creating 3D point clouds which in turn are georeferenced, classified, and cleaned to produce a highly accurate and detailed digital terrain model (DTM). Different visualization techniques further applied to the DTM geotiff file provide insights to the landscape abnormalities which in turn combined with the geophysical and extensive survey can give potential sites of archaeological interest. Close range aerial photogrammetry can be implemented using a camera payload to the UAV. Photographs at low altitude from the ground are used in order to create an orthomosaic of the surface. The orthomosaic is a photogrammetrically orthorectified image product mosaicked from an image collection, where the geometric distortion has been corrected and the imagery has been color balanced to produce a seamless mosaic dataset.

Magnetic prospecting consists of one of the main tools for locating and mapping concealed ancient features. Due to the fact that the earth's magnetic field is precisely recorded in great spatial detail, antiquities in the subsurface disturb this magnetic homogeneity, creating detectable anomalies within the survey data. Magnetometry can be an effective method for delineating soil features such as ditches, pits, and trenches, and it can be used to produce anomalous magnetic field maps reflecting weakly magnetized structures such as wall foundations, providing images of architectural remains that can work complementary and in correlation with those created from aerial survey (photogrammetry & LiDAR) (Tsokas et al., 2012).

Each of the individual methods applied to the research area is non-intrusive providing a way to connect the divide, between surface evidence and the hidden remnants of history under the surface subsequently enhancing our understanding of the past. The integration of the different approaches into a combined platform and visualization surpasses traditional visualization methods using enhanced interpretation through the application of machine learning techniques in image analysis. Data fusion in this work is realized based on the curvelet transform and its great advantage over other types of fusion techniques is that it allows decomposition the unwrapping of the images, to a four-dimensional space, where, in addition to the existing spatial coordinates, they are also expressed as a function of the wavelength and the angle of imaged features (Candes and Donoho, 1999; Karamitrou et al., 2019). Image fusion offers a high potential for the multimethod approach in maximizing the obtained information and increasing the reliability of the interpretation in the detection of archaeological targets. In both cases general, the curvelet-based fusion method (Fig. 1) offers a more complete representation of the investigated areas, incorporating all useful information of the initial images revealing identifying possible archaeological targets.

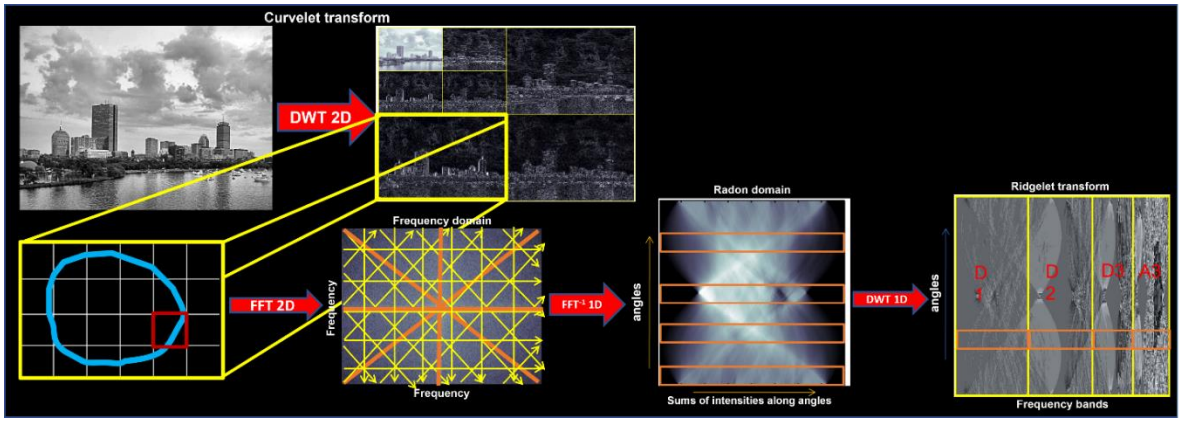

Figure 1. Curvelet Transform Method. ***We begin by applying a discrete wavelet transform to the initial image (top left), dividing it into sub-bands. Each sub-band is then further divided into equal-sized tiles (bottom left). Next, a 2-D Fast Fourier Transform is applied to each tile, expressing the image in the frequency domain. This domain is subsequently partitioned into various slices or angles. Each slice undergoes an inverse FFT, transitioning into the Radon domain. Within the Radon domain, a Ridgelet transform is constructed by applying a 1-D discrete wavelet transform to the slices.***

Through using a combination of techniques during data collection and data fusion in analysis, processes can be efficiently streamlined deriving a larger range of results achieving savings in both time and cost in comparison to relying on conclusions based on individual methods. Another important aspect can be found in the enhanced accountability provided through data fusion where different aspects expressed in images, DTM, orthophotographs, magnetometry, satellite, are improved while presented in a single resulting image that can be analysed further at different scale depending on the research scope of the study. Continuous advancements in technology and research have made photogrammetry, LiDAR survey, and magnetometry more accessible and effective revolutionizing archaeological research by providing new insights and methodologies such as the work presented here.

This project explores the feasibility and practicality of combining images generated through different methods, magnetometry, satellite imagery, photogrammetry and LiDAR data, using various fusion techniques. The use of aerial technology and advanced geospatial techniques in archaeological research is a powerful approach that can provide valuable insights into cultural heritage preservation and management. The ultimate goal of fusion algorithms is to merge all relevant information from the original images into a single image while minimizing background noise.

2. MATERIALS & METHODS

2.1. STUDY AREA

The coastal zone northern to the modern town of Pylos, Messenia, Greece constitutes a landscape of incomparable beauty and particularly great historical, archaeological and environmental importance[1]. The Navarino Bay, the Yialova lagoon, the bay of Voidokoilia dominate the scenery together with the long mountain ranges to the west, including the island of Sphakteria, the Koryfasio peninsula and the hills of Prophitis Ilias and Koukouras (Korres, 2012). The famous sandy beach of Voidokoilia cove, most probably was the harbour of Nestor, king of Pylos where Telemachus arrived when searching for his father Odysseus according to Homeric poems. The Mycenaean Tholos tomb (1680-1600 BC) that is thought to belong to King Nestor's son, Thrasymedes, dominates the cove's north promontory upon the ruins of earlier inhabited phases that go back to the Final Neolithic period (4500-3100 BC) (Marinatos, 1961; Marinatos, 1958; Korres, 1980; Korres, 1981; Korres, 1982). Traces of Neolithic occupation (4500-3100 BC) have been also identified in the so-called "Cave of Nestor" (Korres, 2014), on the cove's south promontory, northern part of the Koryfasio peninsula, now dominated by the Frankish castle known as Palaiokastro or Paleokastro or Paliokastro or Palionavarino[2] (AD 1282/1289). The castle constructed on the ruins of classical Pylos also located here and flourished periodically until Roman times, as it is attested from the

[1] The area is part of the declared archaeological site of Gialova (Government Gazette AAP/284/11-09-2012) and is also environmentally protected as it is part of the NATURA 2000 Protection Network

[2] Paliokastro or Palionavarino translated to 'Old Castle' in order to be distinguished from the new one 'Niokastro' that was built by the Ottomans in 1753 on the south entrance of the Navarino Bay

finds of the trial trenches that Professor S. Marinatos carried out on the peninsula in 1958 (Marinatos, 1961) and mainly from the town's cemetery excavated on the sand bar that separates the Yialova lagoon from the Navarino bay (Gialouris, 1965; Gialouris 1966) and on the east edges of the Profitis Ilias hill (Kaltsas, 1981; Kaltsas 1982; Kaltsas 1990).

The five-year research program entitled "Pylos Geoarchaeological Program – GEAPP" (http://geapp.uop.gr/) began activities in 2021. Among the goals of the Program that stand out are landscape reconstruction, the use of new technological tools for archaeological and environmental research, to inform local authorities about the rich cultural heritage and the special ecosystem, while contributing to the balanced and sustainable development of the area in collaboration with all the environmental, tourism, cultural, productivity organizations locally involved.

From 2021 to 2023 extensive surface survey has been conducted for locating sites and artefacts significant to the research goals of the project. Geodetic technologies are extensively used aiming to transform the program into a digitzed survey providing seamless feed of data to the developed geodatabase for their quantitative, qualitative and spatial analysis. The findings (movable – immovable) are recorded in the geospatial database, are classified and referred, based on a consecutive numbering, which additionally includes the initials of the member of the field team and the square of the design canvas in which they belong.

The surface survey is combined with the surveying of the study area using an Unmanned Aircraft System (UAS). The extensive and detailed photography aims to create a high-precision georeferenced background in the form of an orthomosaic. The aerial survey is completed, corrected and georeferenced with an accuracy of a few millimetres using fixed control points (ground control points - GCPs) that are placed, and their locations measured using GPS GNSS receivers before UAS flight.

The work presented here focuses on two land plots located in the wider study area, plot A east of Prophitis Ilias hill and plot B to the roots of "Koukoura Hill" (Fig. 2). During the 2020-2021 research period the extensive surface survey resulted in a considerable amount of collected pottery, representative of the Late Classical and Byzantine periods in Plot A. A key factor for the selection of the site was the large amount of pottery collected, indicative of the use of the site during the respective time periods even though no immovable monuments were identified which most probably were partially or completely destroyed mainly by agricultural work. Additionally, the short distance, less than 300m, from the excavated Hellenistic cemetery to the southeast, which constitutes Plot B of the geophysical survey, raised hopes about the possible existence of architectural remains at a greater depth. The absence of architectural remains may indeed be related to agricultural operations that destroyed evidence of both human activity in the area as well as remains that could have been found during the surface research.

Plot B is in the area where the Hellenistic cemetery was found in 1981 during ploughing resulting in the rescue excavation realized by the Ephorate of Antiquities of Olympia and the archaeologist N. Kaltsas (Korres et al., 2014; Gialouris, 1965). Twenty-three (23) graves were revealed of deferent types such as cist graves, pyres, jar burials covering an area of around 1000 sq. meters in the tumulus form. The variety of the offerings have been characterized as megarian bowls, white lagynoi, kantharoi, unguentaria, jars, lamps, bronze strigils and knives as well as, bronze and silver coins The cemetery was in use from the 4th century BC until the 4th century AD and the majority of the graves are dating between the 2nd century BC and the 1st century AD. The deceased most probably originated from the Pylos settlement that is situated in the Koryfasio peninsula. The choice of the location was based on the findings detected during the surface survey. In particular the structures that were identified further east of the excavated tombs which, from a first glance and based on the collected pottery, date to the Roman period, perhaps even later. In addition, the tombs excavation in the 1980s was a rescue excavation and therefore spatially limited, subsequently providing no insights on the possibilities of extended archaeological remains in the wider area. The utilization of the geophysical survey in correlation with the LiDAR aerial survey can provide more information for what could be found in the Plot.

2.2. METHODS IMAGING TECHNIQUES

A combination of close-range aerial surveying and satellite imaging techniques were used to provide detailed interpretation of the surface of the two plots under investigation during the 2022-2023 survey period (Zacharias et al., 2023). The close-range aerial survey included aerial photogrammetry and LiDAR scanning (also known as airborne laser scanning or ALS) resulting in the production of a high resolution orthomosaic and digital surface model. Aerial photography and scanning of the area with Light Detection and Ranging (LiDAR) was carried out using an Unmanned Aircraft System (UAS) with two different payloads, specifically, the DJI Matrice 300 RTK quadcopter equipped with the Zenmuse P1 camera and the 3DT Scanfly LITE X Lidar. For the georeferencing of the data, the RTK unit of the UAV was used.

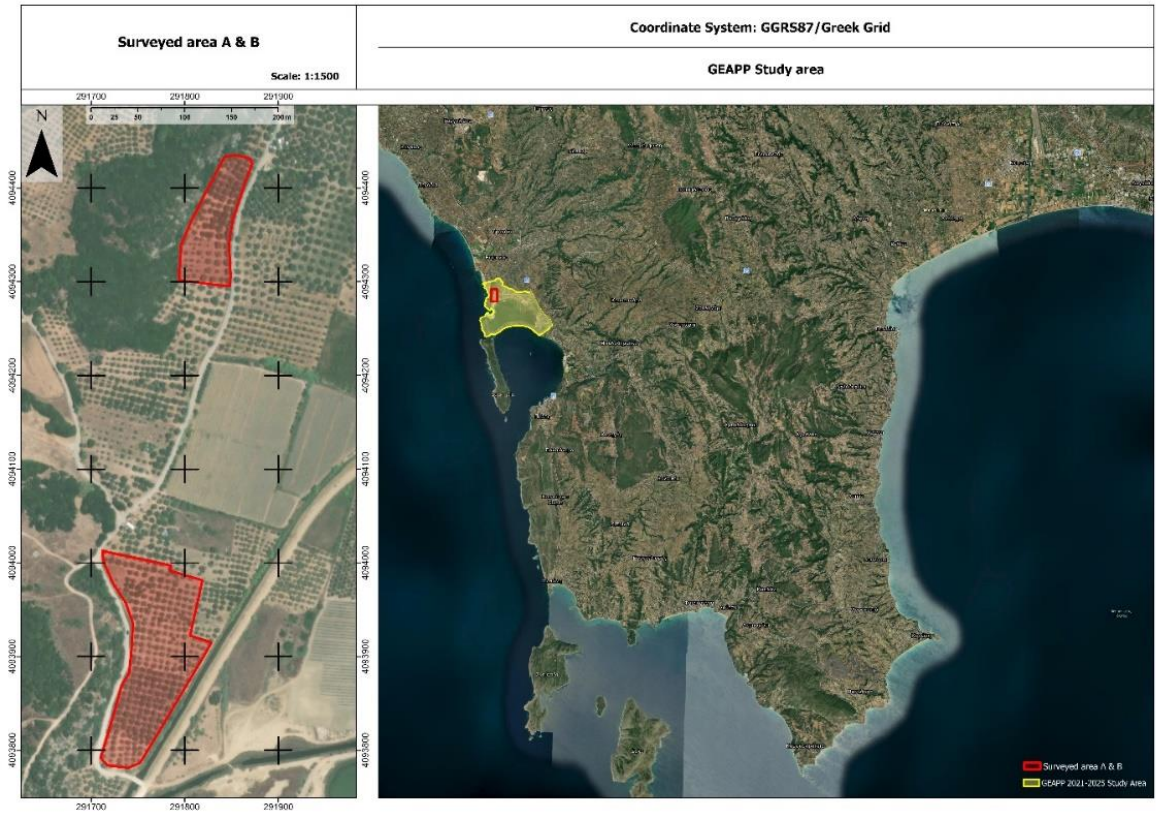

Figure 2. GEAPP study area, plots A & B where the selected imaging techniques and fusion methods are applied

For the purpose of photogrammetry and LiDAR scanning, four flights were conducted at an altitude of 60 meters above ground level while following the terrain. Specifically, two flights were carried out utilizing the Zenmuse P1 camera, and two additional flights were carried out using the 3DT Scanfly LITE X Lidar, paired for each plot. The P1 camera resulted in the capture of 233 photos to facilitate mapping of the area of Plot A and 202 photos for Plot B.

Respectively LiDAR scanning of Plot A resulted in 53,575,319 points captured with a point spacing of 0.066 and surveyed Plot B in 10,306,386 points captured with a point spacing of 0.078.

The georeferenced dense point cloud generated through the ALS method was pre-processed using NAVsolve and SmartProcessingLIDAR software native to the specific LiDAR model. The primary step consists of interfacing the lidar data with the INS data in order to create a single cloud that reaches the manufacturer's accuracy and precision. The next step is to georeference the point cloud and identify the stripes from the point clouds that compose the total mapped area. This specialized software used to align the point cloud strips and determine the coordinate metadata of the points. The dense point clouds are then classified using ArcGIS Pro software. During the first stage of processing, point cloud classification was employed to clear and extract ground elements. The key output of this process was the digital terrain model (DTM), which obtained by the method of triangulation of the ground points and shown in Fig. 2. The results that can be obtained from the study of DTMs is the morphology of the terrain in combination with the differences in elevation. All data collected was processed using the Greek projection system GGRS ’87. In order to create a raster where terrain variations as well as elevation changes are clearly visible, the visualisation with colour gradients of the digital terrain models is applied. The visualized DTM and the orthomosaic are projected as georeferenced layers and resulting gridded layouts through the ArcGIS Pro environment.

One significand factor affecting the final results is the accuracy of the Inertial Navigation System (INS) which is a navigation system that uses accelerometers and angular velocity meters to estimate the position, velocity, and attitude of a moving object. The 3DT Scanfly LITE X INS's accuracy for pitch and roll is 0.03° in real-time. Similarly, the accuracy for heading is 0.08° in real-time, indicating that the INS can estimate the pitch, roll and heading angles of the object with high accuracy.

Geophysical survey

The survey, realized in the field, consisted of measurements taken along parallel traverses. Measuring tapes placed on the ground at 0.5m intervals created a subsidiary grid within each grid square. The grid

was in the Greek projection system GGRS ’87 in real time using a GPS GNSS base and rover system. The rover receiver was mounted to the magnetometer (Fig. 3) while the base receiver remained mounted on a tripod over a known point correcting consistently the location of the rover receiver ensuring high accuracy in the georeferencing of the model.

Figure 3. Magnetometry survey Plot A.

FUSION TECHNIQUE

The fusion method used in this work is based on the curvelet transform (Karamitrou et al., 2019), an operation based in two decompositions; the Radon transform (Radon, 1917), which transforms an image into a series of line integrals along various orientations, and the Ridgelet transform (Logan & Sheep, 1975; Candes, 1998; Candes & Donoho, 1999; Asano, 2002), which is the application of 1-D wavelet transform to the line integrals of the Radon transform. The curvelet decomposition, transforms a 2-D image into the 4-D space, whereas mentioned above, in addition to the two spatial coordinates, it is also expressed as a function of the space and the orientation.

If an image is represented as a bivariate function $f(x_1, x_2)$, then its Ridgelet transform $\Re_f$, can be expressed in relationship to the Radon transform R_f (Candes, 1998; Candes & Donoho, 1999) as,

$$\Re_f(a, b, \theta) = \oint_{\mathbb{R}} \psi_{a,b}(t) R_f(\theta, t) dt$$

Where $\psi_{a,b}(t)$ is a wavelet-type univariate function,

$\psi_{a,b}(t) = \psi(\frac{t-b}{a})$. In the given equation $a > 0$ represents the scale, $b \in \mathbb{R}$, the location along t, and $\theta \in [0,2\pi]$ its orientation.

Note that as the Radon transform computes projections of f alonh radial lines defined as

$$\cos(\theta)x_1 + \sin(\theta)x_2 = const,$$

the Ridgelet transform can be considered as the application of the wavelet transform on the different projections of f.

The ridgelet coefficients describe with great accuracy linear features in the image. However, if the image contains curved lines and features then it fails to describe them correctly. One of the main advantages of curvelet transform is that before the application of the ridgelet transform it separates the image into equal size tiles. This procedure helps in representing the curved features as almost straight lines (Fig. 4). This method helps all features to be efficiently and effectively represented by ridgelet transform.

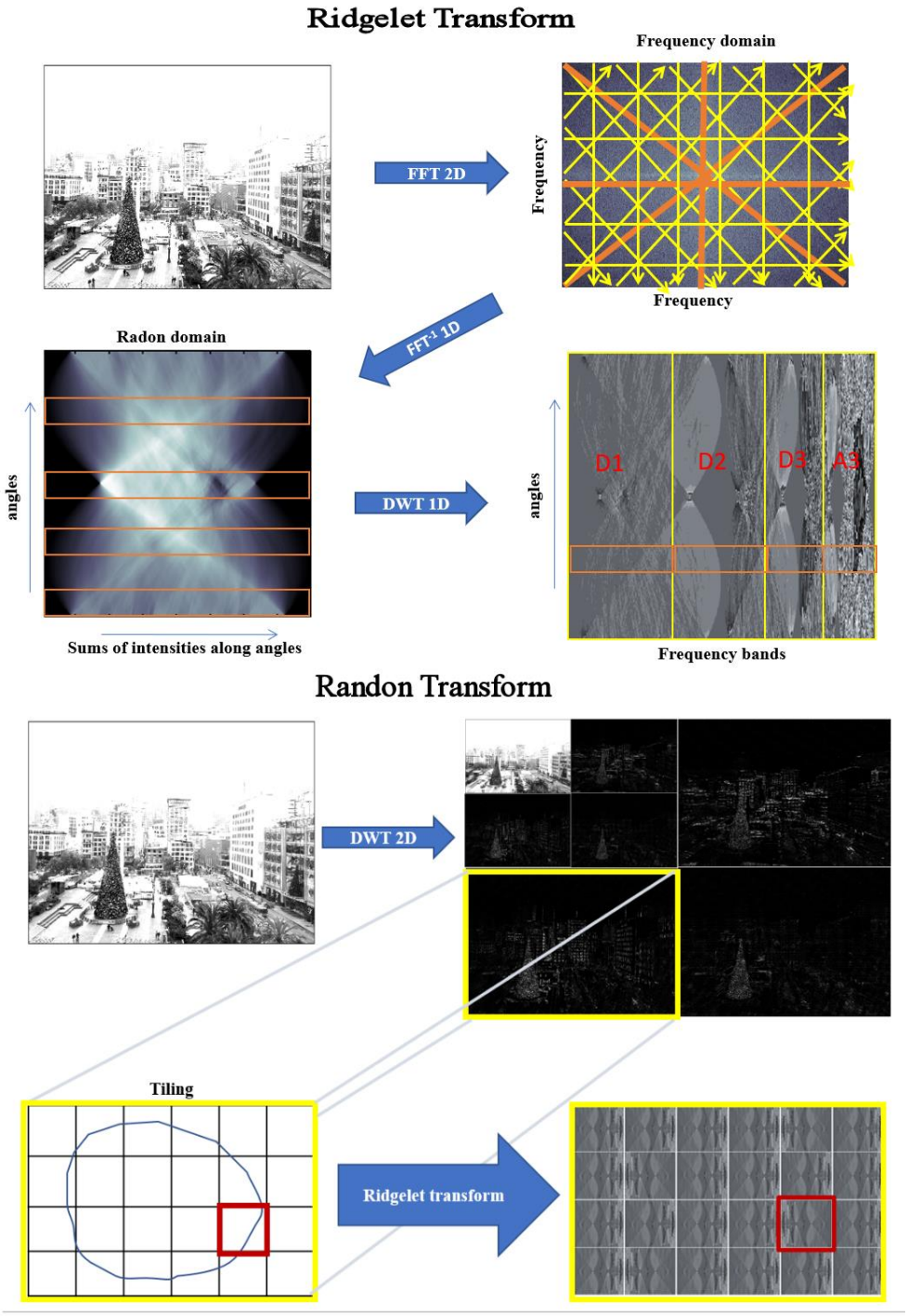

Figure 4. Graphical representation of the curvelet decomposition algorithm. Top image shows the ridgelet transform, where to the initial image a 2-D Fast Fourier transform (FFT) is applied, expressing the image in the frequency domain. With the application of the 1-D Discrete Wavelet transform we move to the ridgelet transform. The bottom image explains the ridgelet transform. A 2-D discrete wavelet transform is applied to the initial image decomposing it into different sub-band levels. On each level tilling is applied so that curved features can be represented as almost straight lines within each tile. Finally, on each tile the ridgelet transform is applied yielding the curvelet coefficients.

Fig. 5 is a schematic presentation of the steps followed by the curvelet transform algorithm. Image A and image B are the two initial images that both images undergo an initial decomposition into sub bands using the 2-dimensional discrete wavelet transform. Subsequently, the details within each sub band are further divided into smaller tiles and the curvelet coefficients are generated by applying the ridgelet transform to each tile within each sub band. The curvelet transform offers an advantage by expressing

the image as a function of scale (via the wavelet transform), orientation (through the ridgelet transform), and spatial location (via tiling) of its features.

The subsequent step involves combining these curvelet coefficients from the original images to create a fused image in the curvelet domain. Following this, the maximum frequency rule is applied to select features that offer the best representation from the initial images.

Finally, the inverse curvelet transform is applied to extract the final fused image. This inverse process essentially reverses the initial decomposition, resulting in the reconstructed fused image.

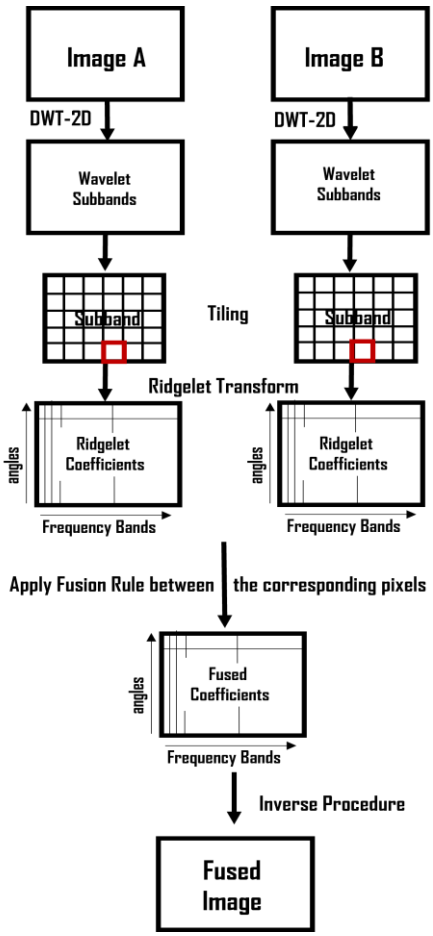

Figure 5. Schematic representation of the Curvelet Transform algorithm.

3. RESULTS & DISCUSSION

3.1. PHOTOGRAMMETRY RESULTS

Regarding the photogrammetry data processing, specialized software dedicated to unmanned aerial systems (UAS) mapping was used to create a georeferenced dense point cloud. Specifically, Agisoft Metashape photogrammetry software was used to produce the orthomosaic, which is shown in Fig. 6 and Fig. 7, utilizing the point cloud data. The complete orthomosaic for each plot resulted in the generation of a high-resolution georeferenced aerial photo with the true color of the surveyed area. By comparing the orthomosaic with the DTM visualization, changes in the terrain can be accurately identified and documented.

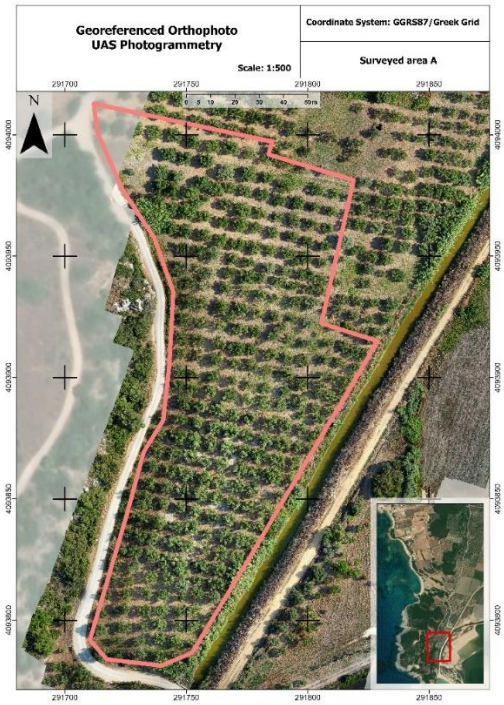

Figure 6. Georeferenced Orthophoto – UAS Photogrammetry (Surveyed area A).

Figure 7. Georeferenced Orthophoto – UAS Photogrammetry (Surveyed area B).

3.2. LIDAR RESULTS

The level of detail of the generated DTM depends on the density of the points in the scan. In the case of an archaeological site study, a greater density of ground points is required. The use of the 3DT Scanfly LITE X Lidar and ArcGIS Pro software for point cloud classification and DTM generation is a highly effective approach in accurately capturing and analyzing the terrain of a surveyed area. By employing various filters, including noise, classification, and ground classification filters, vegetation points are removed, and ground elements are isolated and extracted to produce a highly accurate and detailed DTM (Štular et al., 2021).

The resulting DTM provides a clear picture of the variations in elevation of the surveyed area, highlighting any changes in terrain. The accuracy of the DTM can be evaluated through cross-validation with GCPs and visual inspection, which demonstrate a high degree of accuracy and precision, with a root-mean-square error (RMSE) of less than 5 cm. The Shaded Relief map is a visualization tool that provides a three-dimensional representation of the terrain and contours as shown in Fig. 8 and Fig. 9. This map simulates the shadows and highlights that would be created by a hypothetical light source, creating a realistic and accurate depiction of the surveyed area, revealing features with low light source on flat areas such as in the two plots of this study.

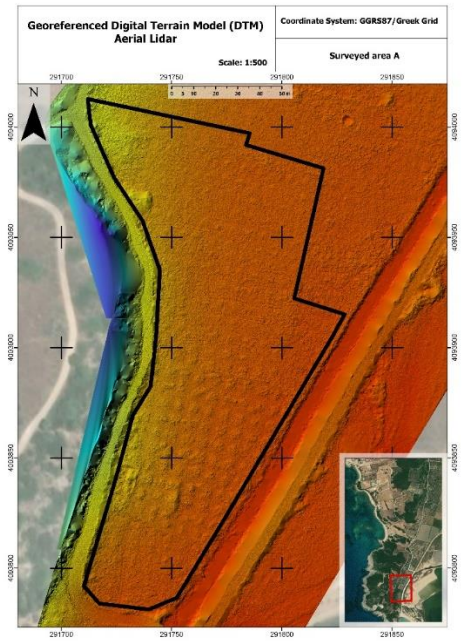

Figure 8. Digital Terrain Model (DTM) – Aerial Lidar (Surveyed area A)

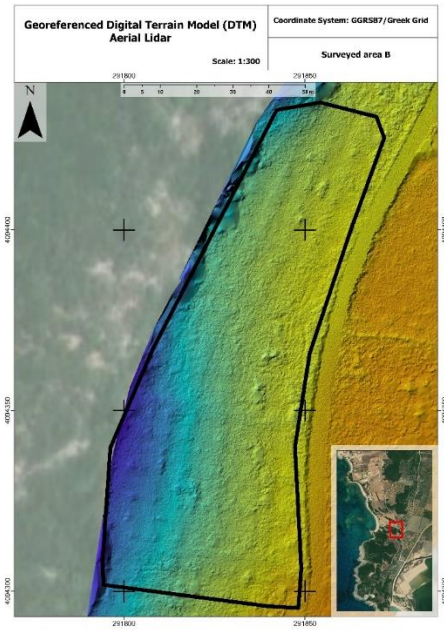

Figure 9. Digital Terrain Model (DTM) – Aerial Lidar (Surveyed area B)

The 3DT Scanfly LITE X Lidar module captured precise point cloud data, penetrating through the vegetation, capturing points on the ground, to create a dense and highly accurate map of the site. Meanwhile, the P1's high-resolution camera and 3-axis stabilized gimbal allowed for the capture of detailed images from multiple angles, resulting in a highly detailed and accurate orthomosaic of the area. The 3DT Scanfly LITE X Lidar module can capture data with an accuracy of up to 5 cm and 3cm precision, while the P1's 45-megapixel full-frame sensor captures highly detailed images with exceptional color accuracy and low noise, achieved a Ground Sample Distance (GSD) of 0.75 cm per pixel at a flight altitude of 60 meters. Both sensors also feature advanced synchronization technology, ensuring accurate geotagging of captured data. The selection of those modules in the Pylos Geoarchaeological Program's case study was based on the morphology of the surrounding terrain and the necessary vegetation removal required for the final maps.

3.3. MAGNETOMETRY RESULTS

Fig. 10 presents the magnetometry results for the two plots. The magnetic survey conducted in the area for this study has yielded valuable insights into subsurface features and anomalies. As part of the investigation, testing trenches are being employed to further examine the geophysical survey results on-site. This iterative process will continue into the upcoming excavation season, enhancing our understanding of the archaeological landscape.

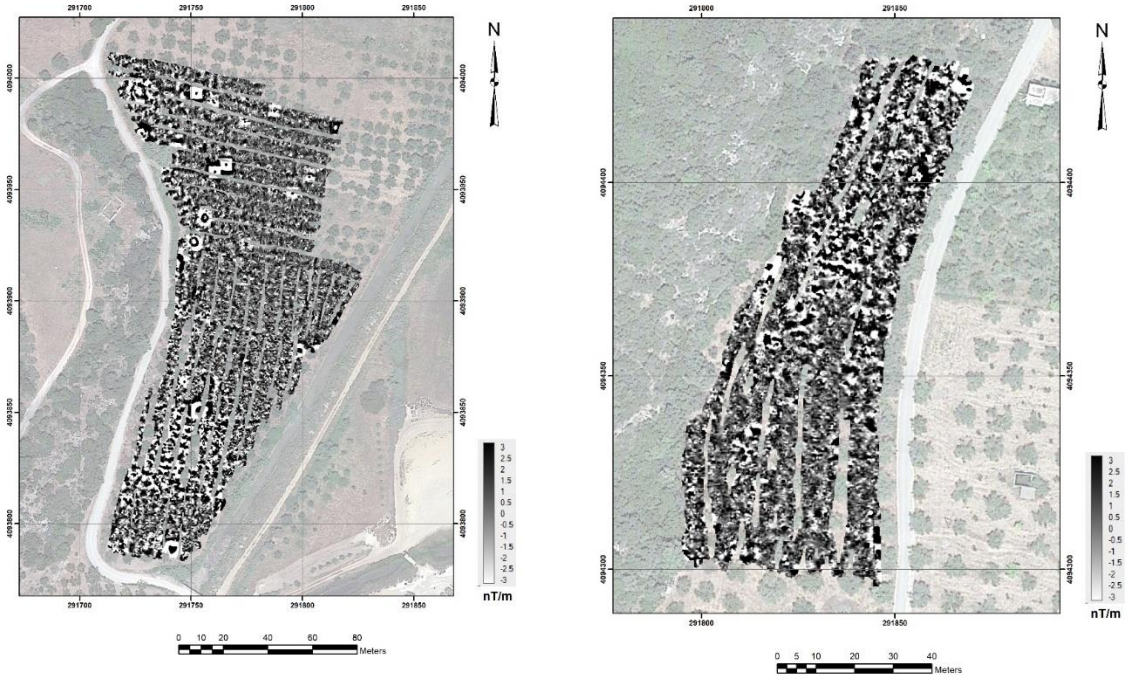

Figure 10. Magnetic anomaly maps Plot A (left) and Plot B (right)

3.4. CURVELET TRANSFORM RESULTS

The results of the study provided a case depended on methodology aiming to a better resolution and accuracy of the spotted antiquities and therefore towards a successful management of the area, safeguarding and promoting buried antiquities.

Image fusion holds great promise for employing a multi-method strategy to optimize information extraction and enhance the dependability of interpretation during the detection of archaeological targets. In both scenarios, utilizing the fusion technique based on curvelets provides a more comprehensive portrayal of the surveyed regions, merging all relevant details from the original images to reveal potential archaeological targets.

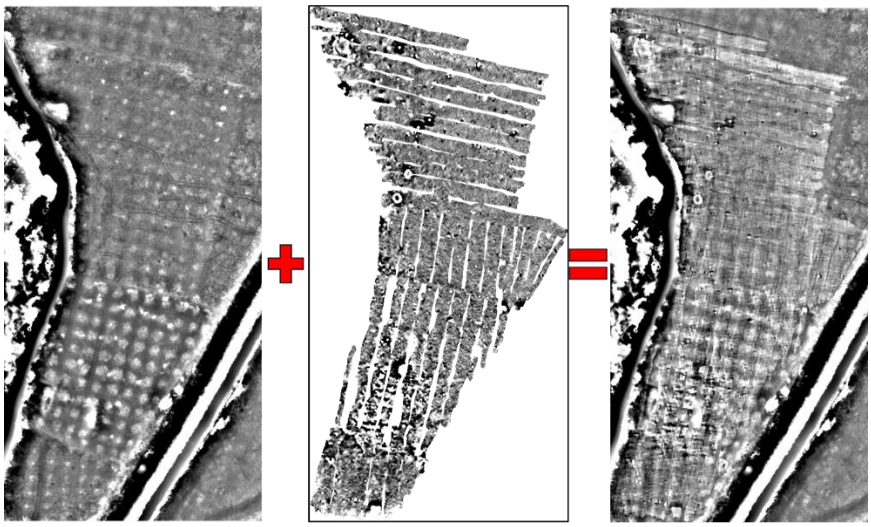

Figure 11. DTM derived from LIDAR after removing the long wavelength variations + magnetic gradiometry image = fused image (Area A).

In the LIDAR image, the vegetated areas are presented with white dots while in the magnetic image, there is no information along their linear projection due to the inability of the instrument to take measurements in these areas (Fig. 11). In the aerial image the

process of removing these large wavelength anomalies was performed the first instance manually using image processing applications using MATLAB. In the fused image although these features were considered as noise and during the fusion process this information should have been removed as there was an absence of geophysical information on these areas no fusion was applied between these non-overlapping parts of the images. This resulted in a final fused image with noise in these areas covering up possible features that might be present.

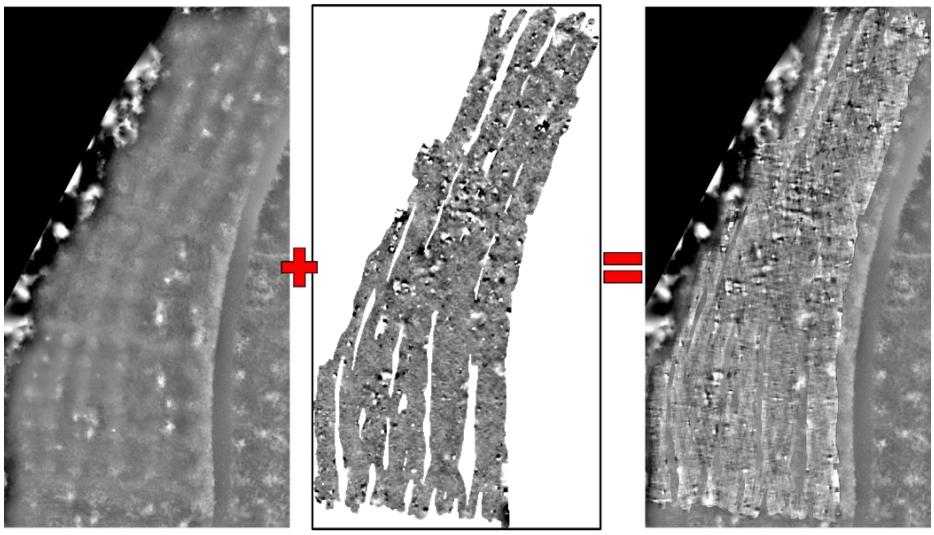

Figure 12. DTM derived from LIDAR after removing the long wavelength variations + magnetic gradiometry image = fused image (Area B).

The presence of tree fields is clear in Area B as well, but not as intense as it was in Area A resulting in a clearer final fused image (Fig. 12). This means that the fusion was extended in most of the overlapping areas of the two images. Nevertheless, we still have areas with no information on the geophysical image due to the presence of vegetation. In the final fused image, both images were combined meaning that in the areas where the geophysical image had no information it was provided by the aerial images creating a final complete image that includes all available information.

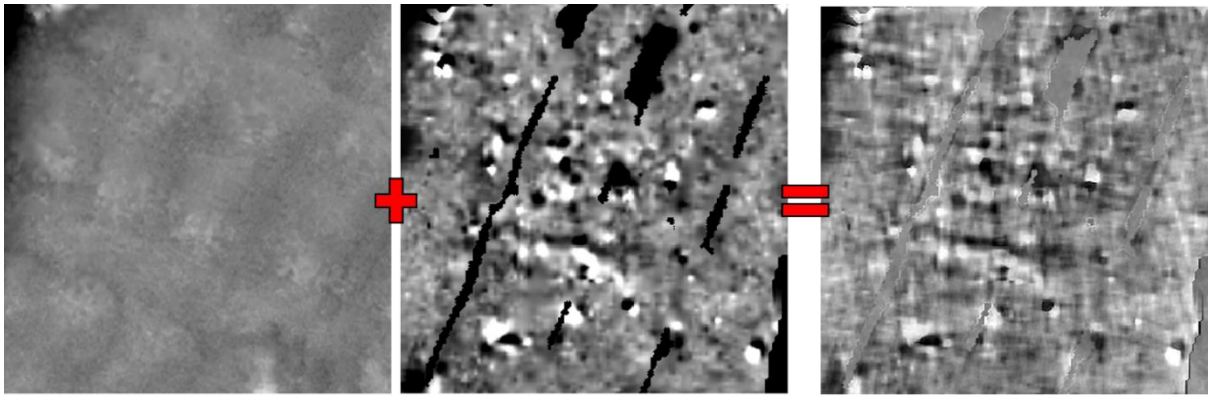

Figure 13. Zoom part of the Area B. (Left) zoomed part of the aerial image produced using UAS, (middle) zoomed part of the magnetic image (vertical gradient of the local magnetic field) and (right) the respective zoomed part of the fused image with the use of the curvelet transformation method giving emphasis at north-east to south-west orientation.

However, in the fused image the noise is suppressed while the interesting features appear enhanced and, in many cases, more complete. Fig. 13 is a zoomed part of the Area B where a rectangular feature at the centre of the image that is visible only in the magnetic image can be see clearer and better defined in the final fused image. This is because during the fusion process the noise is supressed, and the interesting features were enhanced creating a final image with more distinct characteristics and clear targets.

4. CONCLUSIONS

Data fusion between different types of sensors is an important and useful tool for the analysis of overlapping data and for recognizing and mapping geological archaeological structures before their excavation.

One main advantage is that it allows a more complete interpretation of the data by combining anomalies provided by different sensors that may have different sensitivity-oriented characteristics regarding their special resolution, contrast, size, geometry, etc. For this reason, the curvelet transform provides an excellent tool as it can represent efficiently and effectively both linear and curve-linear features with different characteristics, scales, and orientations. Additionally, it establishes the means for objectively selecting the best features to be included in the fused image, for example by using the maximum frequency rule as we showed in this work. Moreover, it allows to treatment in a different way features of different scales and/or extent along different orientations, giving the ability to suppress the noise based on prior information. This can be particularly useful in cases where the images contain systematic noise (e.g., plowing lines, microtopography) or it is necessary to select between archaeological features of different era.

In this work, two different locations of the archaeological area of Pylos, Messenia in South Greece were examined. In both areas, the final fused image produced a more complete representation of the areas of investigation as they managed to combine all the interesting features from each of the initial images independently. In the final fused images, the noise (systematic and random) is suppressed as much as possible, and the representation of potential targets has been improved significantly. However, as noted above, the presence of olive trees and other types of vegetation in both areas presented a challenge as the geophysical instrument was not able to cover these areas resulting in large linear zones with no information. On the other hand, in the aerial images, these areas were presented as white dots.

Nevertheless, in some cases, structures that are segmented in the initial images are shown complete in the fused image, something that helped their detection and the further interpretation/identification. Additionally, in some cases some rectilinear features which are either not clear or are visible in one of the two initial images through the fusion process in the final combined image look complete and more distinct. This can help archaeologists in having a more comprehensive image of the investigated sites by identifying areas of possible historical and cultural interest.

It should be noted that the fused image is a powerful, additional tool that can further help the interpretation of the data and does not intend to replace the initial images during the analysis. Additionally, more than one fused image can be produced, each one focused on enhancing or smoothing selected features over others. For example, in cases where multiple targets are imaged, and the result is dense then the information needs to be separated for interpretation reasons.

Author Contributions: Investigation, resources, visualization, data curation, writing—original draft preparation: A. Karamitrou, A. Kazolias, V.V.P.; Writing—review and editing, supervision & project administration: G.N.T., N.Z., E.M.; Conceptualization, methodology, validation: A. Karamitrou, A. Kazolias, V.V.P., M.K, A.S., G.N.T., N.Z. All authors have read and agreed to the published version of the manuscript.

ACKNOWLEDGEMENTS

The authors gratefully acknowledge financial support from ARISTEAS project. The project was implemented within the scope of the "Exceptional Laboratory Practices in Cultural Heritage: Upgrading Infrastructure and Extending Research Perspectives of the Laboratory of Archaeometry", a co-financed by Greece and the European Union project under the auspices of the program "Competitiveness, Entrepreneurship and Innovation" NSRF 2014-2020.

REFERENCES

Asano, A. (2002) Radon transformation and projection theorem. *Topic 5, Lecture notes of subject Pattern information processing, Autumn Semester*, http://kuva.mis.hiroshima-u.ac.jp/~asano/Kougi/02a/PIP/.

Candes, EJ. and Donoho, DL. (2000) Curvelets–a surprisingly effective non adaptive representation for objects with edges. *In A. Cohen, C. Rabut, & L. Schumaker (Eds.), Curves and surface fitting*. Saint-Malo, Nashville, TN: Vanderbilt University Press, 105–120.

Candes, E.J. (1998) Ridgelets: theory and applications. *Ph.D. Thesis*, Department of Statistics, Stanford University

Candes, E.J. and Donoho, D.L. (1999) Ridgelets: a key to higher- dimensional intermittency? *Roy Soc of London Phil Tr A*, 357, 1760-2495.

Drapa, P., Sgrenzaroli, M., Canciani, M., Cannata, G. and Seinturier, J. (2003) Laser Scanning and close-range photogrammetry: Towards a single measuring tool dedicated to architecture and archaeology, *CIPA XIXth INTERNATIONAL SYMPOSIUM*, Turkey. pp.1-6.

Gialouris, N. (1965) The Hellenistic cemetery of Gialova - Palaionavarino, ΑΔ 1965, *Chronicles,* p. 204-205. (in Greek)

Gialouris, N. (1966) The Hellenistic cemetery of Gialova - Palaionavarino, AD 21, *Chronicles*, p. 164-165. (in Greek)

Giacomo, P., Gómez, A., Adineh, A., Rahrig, M., and José Luis Lerma (2022) 3D Data Fusion for Historical Analyses of Heritage Buildings Using Thermal Images: The Palacio de Colomina as a Case Study, *Remote Sensing 14*, no. 22: 5699.

Grammer, B., Draganits, E., Gretscher, M., and Muss, U. (2017) LiDAR-guided Archaeological Survey of a Mediterranean Landscape: Lessons from the Ancient Greek Polis of Kolophon (Ionia, Western Anatolia). *Archaeol. Prospect*., 24: 311–333. doi: 10.1002/arp.1572.

Henry, Edward R., Alice P. Wright, Sarah C. Sherwood, Stephen B. Carmody, Casey R. Barrier, and Christopher Van de Ven. (2020) Beyond Never-Never Land: Integrating LiDAR and Geophysical Surveys at the Johnston Site, Pinson Mounds State Archaeological Park, Tennessee, USA, *Remote Sensing 12*, no. 15: 2364.

Kaltsas, N., AD 36 (1981), Hellenistic cemetery in Gialova-Paleonavarino.*Chronicles*, p. 152, (in Greek)

Kaltsas, N., AD 37 (1982), *Chronicles*, p. 137. (in Greek)

Kaltsas, N. (1990) From the Hellenistic cemetery of Pylos AD 38, *Meletes*, p.1-77. (in Greek)

Karamitrou, A., Bogiatzis, P. and Tsokas, G. N. (2020) Fusion between Geophysical and Satellite images for the study of Archaeological sites. *Archaeological Prospection*, 27, 119–133.

Kadhim, I.; Abed, F.M. A (2023) Critical Review of Remote Sensing Approaches and Deep Learning Techniques in Archaeology. Sensors 2023, 23, 2918. https://doi.org/10.3390/s23062918

Korres, G. (2012) Messenia Historical and Archaeological Outline, *Prehistoric Times*. p. 427- 447 edn. Melissa (in Greek)

Korres, G.S. (1980) Excavations in Pylia PAE 1980, p. 150-175. (in Greek)

Korres, G.S. (1981) Excavations in Pylia PAE 1981, p. 194-239. (in Greek)

Korres, G.S. (1982) Excavations in Pylia PAE 1982, p. 191-230. (in Greek)

Korres, G.S., Sampson A., Katsarou S. (2014) Nestoras Cave in Voidokoilia Pylos, the investigation and preliminary investigation of older and newer findings, *Proceedings of the 4th Local Conference of Messenian Studies*. p.49-50. (in Greek)

Logan, B. F. and Shepp, L. A. (1975) Optimal reconstruction of a function from its projections. *Duke Math*. J. 42, 4, 645-659.

Marinatos, S. (1961) Excavations in Pylos, *PAE 1956*, p 202-206. (in Greek)

Marinatos, S. (1965) Excavations in Pylos - Coriphasium, *PAE 1958*, Athens, p. 184-187. (in Greek)

Monterroso-Checa, A., Teixidó, T., Gasparini, M., Peña, J.A., Rodero, S., Moreno, J.C. and Morena, J.A. (2019) Use of Remote Sensing, Geophysical Techniques and Archaeological Excavations to Define the Roman Amphitheater of Torreparedones (Córdoba, Spain), *Remote Sensing 11,* no. 24: 2937.

Nikolakopoulos K. G., Soura K., Koukouvelas I. K., Argyropoulos N. G. (2017) UAV vs classical aerial photogrammetry for archaeological studies, *Journal of Archaeological Science: Reports*, Volume 14, pp. 758-773, ISSN 2352-409X, https://doi.org/10.1016/j.jasrep.2016.09.004.

Panagiotidis, V. V. and Zacharias, N. (2022) Digital Mystras: An approach towards understanding the use of an archaeological space, *Scientific Culture*, Vol. 8, No. 3, pp 85 99.

Poirier N.Baleux F, Calastrenc C. (2020). The mapping of forested archaeological sites using UAV LiDaR. A feedback from a south-west France experiment in settlement & landscape archaeology. *Archéologies numériques*. 4. 10.21494/ISTE.OP.2020.0556.

Radon, J. (1917) Uberdie Bestimmung von Funktionen durch ihere Integralwerte Lags gwisser Mnigfalaltigkeiten. *Ber. Verchs. Akad.Wiss. Leipzig*, Math-Nat.K.I, 69, 269-277.

Risbøl O, Gustavsen L. (2018) LiDAR from drones employed for mapping archaeology – Potential, benefits and challenges. *Archaeological Prospection*. 25: 329–338. https://doi.org/10.1002/arp.1712

Štular, B., Eichert, S. and Lozić, E. (2021) Airborne LiDAR Point Cloud Processing for Archaeology. *Pipeline and QGIS Toolbox. Remote Sens.* 13, 3225.

Tsokas, G. N., Tsourlos, P. and Papadopoulos, N. (2009) Electrical resistivity tomography: a flexible technique in solving problems of archaeological research. *In Seeing the Unseen. Geophysics and Landscape Archaeology*, edited by S. Campana and S. Piro.

Tsokas, N. Gr., Moortel, A., Tsourlos, P., Stampolidis, Al., Vargemezis, G., and Zahou, E. (2012) Geophysical Survey as an Aid to Excavation at Mitrou: A Preliminary Report. *Hesperia: The Journal of the American School of Classical Studies at Athens*, 81(3), 383–432.

Vella, M.-A., & Sarris, A. (2022). Geophysical survey in archaeological context: A review from Cyprus. Archaeological Prospection, 29(3), 417–450. https://doi.org/10.1002/arp.1856

Zacharias, N., Militsi, E., Kylafi, M., Valantou, V., Kazolias, A., Kompoti, A. and Panagiotidis, V.V. (2023) Sand & stones: The Pylos Geoarchaeological Program, *Journal of Archaeological Science: Reports*, Volume 51, 104210.